Adjoint Methodologies For Proton Therapy

Bachelor Thesis

Author:
Menno Kasbergen
Student Number: 4371844
Thesis Registration Number:

Supervisors:
dr. Zoltán Perkó
dr. ir. Danny Lathouwers

Committee Members:

Reactor Institute Delft
Section Medical Physics and Technology
Department of Radiation Science and Technology
Faculty of Applied Physics
Delft University of Technology

August, 2018

TU Delft

Abstract

Proton therapy is an advanced, high potential method introduced into radiotherapy as of lately. Protons have a well-defined spot size known as the Bragg peak. Due to this Bragg peak precise treatment with minimal damage to normal tissues can be possible. Planning methods for proton therapy nowadays consist out of slow methods like Monte Carlo Simulation or S_N method. These methods are statistical based and therefore carry statistical uncertainty. To reduce uncertainty one has to run these slow methods over and over again.

Adjoint theory creates an opportunity to calculate response changes without having to calculate the proton transport equation over and over again. This thesis provided a first and critical review of the adjoint proton transport equation. The goal of the thesis is to test the suitability of adjoint theory for calculating proton doses and response changes.

To check if the change in response can be calculated with the help of the adjoint proton flux, we changed the total cross with ±1%, 5% and ±10% and compared this adjoint calculation with the normally used calculation. After plotting the response changes for an adjoint source on the whole space domain and for a local adjoint source around the Bragg peak, we can conclude that the response changes can be calculated accurately with the help of the adjoint proton flux. Calculating response changes with adjoint theory is much faster than forward calculations. Adjoint theory creates an opportunity to do many calculations way faster. With this theory one can treat tumours in the future more accurately. This can improve the future of proton therapy vigorously.

The method that we used needs to be improved before one can apply it into proton therapy clinics: (i) the 3D adjoint proton transport equation from the 3D Boltzmann Fokker-Planck approximation has to be derived to provide more detail and complicity, (ii) a 3D calculation of the adjoint source / tumour is needed for an exact practical representation, (iii) energy that is transferred to secondary particles must be included in the S_N method to create an opportunity for proton therapy calculations in the typical energy range (70MeV-200MeV) and, (iv) to accomplish proton beam adaptions due to movement of the patient (breathing, slight movement of the body), one need to continuously image the patient during treatment.

List of Symbols

Latin Symbols

Symbol	Description	Units
A_n	An indication for operators	[-]
B	1D linear Boltzmann equation	[-]
$B^{\dagger}$	Adjoint 1D linear Boltzmann equation	[-]
E	Energy	[MeV]
$E_{g-1/2}$	Energy on upper boundary of energy group g	[MeV]
$E_{g+1/2}$	Energy on lower boundary of energy group g	[MeV]
ΔE_g	Width of energy group g	[MeV]
E_{max}	Maximum energy of energy domain (boundary condition)	[MeV]
E_{min}	Minimum energy of energy domain (boundary condition)	[MeV]
$f(x)$	A function to define the response at/in some region/point	[-]
l	Depth of penetration in x direction	[cm]
$L^{\dagger}_{CSD}$	Adjoint continuous slowing down operator	[cm^{-1}]
p^A	Basis function ($p^A = 1$)	[-]
p^E	Basis function ($p^E = 2(E-E_g)/\Delta E_g$)	[-]
R	Response of fixed source calculations	
S	Fixed source of protons	[MeV]
$S^{\dagger}$	Adjoint source	[MeV]
$S(E)$	Stopping power	[MeV cm^{-1}]
$S_{g\ +/-\ 1/2}$	Stopping power evaluated at boundaries of energy group g	[MeV cm^{-1}]
$u(x)$	Unit step function: 0 if $x<0$, 1 if $x\geq 0$	[-]
x	Spatial component	[cm]
x_{max}	Maximum depth of tumour	[cm]
x_{min}	Minimum depth of tumour	[cm]

Greek Symbols

Symbol	Description	Units
δ_{ij}	Kronecker delta: 0 if i≠j, 1 if i=j	[-]
$\delta(.)$	Dirac Delta function	[-]
μ	Cosine scatter angle	[-]
π	pi: 3.14159265359…	[-]
σ_t	Total macroscopic scatter cross section	[cm^{-1}]
σ_{tr}	Macroscopic transport cross section	[cm^{-1}]
Σ_D	Response function corresponding to dose factor	[MeV]
$\varphi(x,E,\Omega)$	Angular proton flux at position x, energy E and moving in direction Ω	[cm^{-2} MeV^{-1} s^{-1}]
$\varphi^{\dagger}(x,E,\Omega)$	Adjoint angular proton flux at position x, energy E and moving in direction Ω	[cm^{-2} MeV^{-1} s^{-1}]
$\varphi_{a,i,n,g}$	Average proton flux in spatial cell i, discrete ordinate n and energy group g	[cm^{-2} MeV^{-1} s^{-1}]
$\varphi_{e,i,n,g}$	Normalized slope of flux in spatial cell i, discrete ordinate n and energy group g	[cm^{-2} MeV^{-1} s^{-1}]
$\varphi_{i,n,g}$	Flux in spatial cell i, discrete ordinate n and energy group g	[cm^{-2} MeV^{-1} s^{-1}]
Φ_E	Energy flux	[MeV s^{-1}]
Ω	Direction of motion	[-]

Table of Contents

1. An Introduction to Proton Therapy

1.1. Treating Cancer with Radiotherapy

Cancer is a group of diseases involving abnormal cell growth with the potential to invade or spread to other parts of the body. There are more than two hundred types of cancers. Cancer is the second leading cause of death globally, and was responsible for 8.8 million deaths in 2015. Globally, nearly 1 in 6 deaths is due to cancer. About 40% of cancer patients receive radiotherapy as part of their treatment.

Radiotherapy is a cancer treatment that uses high doses of radiation to kill cancer cells or slow their growth by damaging their DNA. Cancer cells whose DNA is damaged beyond repair stop dividing or die. When the damaged cells die, they are broken down and removed by the body. Radiation therapy does not kill cancer cells right away. It takes days or weeks of treatment before DNA is damaged enough for cancer cells to die. Then cancer cells keep dying for weeks or months after therapy ends. Due to the type of cancer, location of the tumour and the size of the tumour medical experts will choose the type of radiation therapy. There are two main types of radiation therapy, external beam and internal. Radiation beams used in external radiation therapy come from four types of particles: photons, electrons, protons and neutrons. This thesis will focus on proton therapy. [1],[8]

1.2. Proton Therapy

During the past three decades, clinical procedures using highly collimated radiation beams have been used routinely. The main idea in radiation therapy has been to maximize the dose in each point of the tumour, without affecting the surrounding healthy tissue and especially the vital organs like the spine and the liver. The dose received by the healthy tissue and vital organs is usually lower than the dose received by the tumour, since multiple, individually non-lethal beams that intersect at the tumour, are used during treatment.

There are many advanced methods introduced into radiotherapy as of lately. One of the methods is proton therapy, a method with a high potential. The dose distribution of a proton beam is very convenient in radiotherapy and therefore protons might even be a better way to threat tumours than the ‘usual’ used methods like x-rays and electrons [7],[14]. Protons have a well-defined spot size (a few millimetres) with a high dose in that region, also known as the Bragg peak (see figure 1). Beyond the Bragg peak no energy is deposited. A second advantage is that protons do not have a high entrance dose like x-rays or neutrons. This gives an opportunity for a precise treatment with minimal damage to normal tissues. At the Lawrence Berkeley National Laboratory in 1954, they treated the first patient with this ‘new’ therapy. The main challenge during proton therapy is how to adapt the particle accelerator so that the protons are useful for therapy. Protons have a Bragg peak of only a few millimetres, so to treat the tumour one has to spread out the protons along and orthogonal to the beam direction. There are currently two methods of proton therapy: passive scattering and active scanning, which are discussed in chapters 1.1 and 1.2.

To determine the treatment method that is suited best for a particular patient, a computed tomography scan (CT-scan) or a magnetic resonance imaging scan (MRI-scan) is made of the patient's body. With this scan one can determine the geometry of the body. After the scans 3D dose calculations are needed to determine the trajectory of the proton beams and where they deposit the dose.

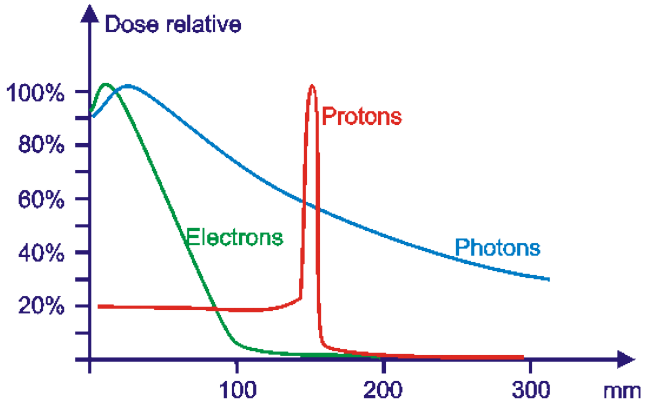

Figure 1: Schematic of dose distribution along a single line for protons vs other types of radiation. [4]

1.2.1. Passive Scattering

In passive scattering techniques, the proton beam is spread by placing scattering material into the path of the protons. A single scattering broadens the beam sufficiently for treatments requiring small fields. For larger fields, a second scatterer is needed to ensure a uniform dose profile. A combination of custom-made collimators and compensators conform the dose to the target volume. The spread out Bragg peak (SOBP) used for treatment is obtained via a set of range modulator wheels or ridge filters inside the nozzle of the delivery system [7].

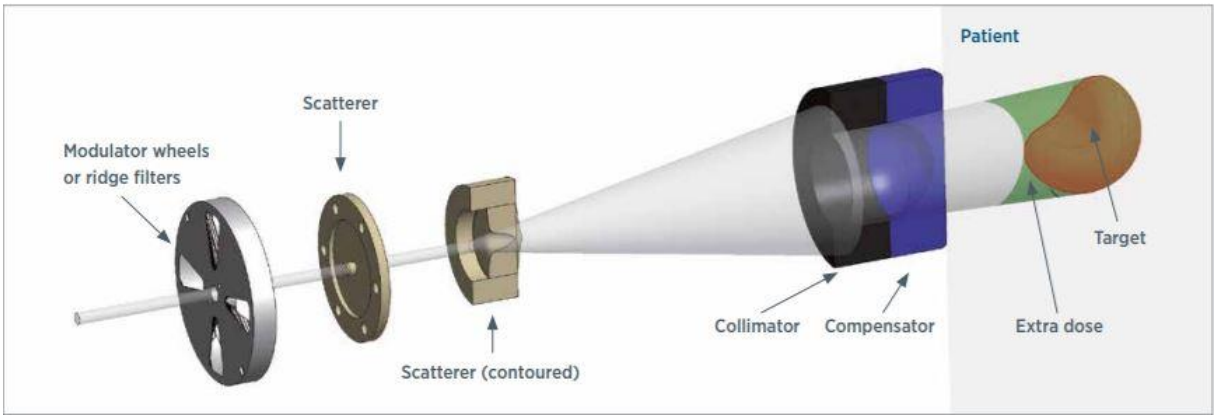

Figure 2: Proton Scattering diagram. [11]

1.2.2. Active Scanning

Active scanning, better known as beam scanning, is based on magnets that deflect and steer the proton beam to the right point. A computer is controlling the narrow mono-energetic beam that scans the volume part by part in one layer. Varying the energy of the beam controls the depth of each layer.

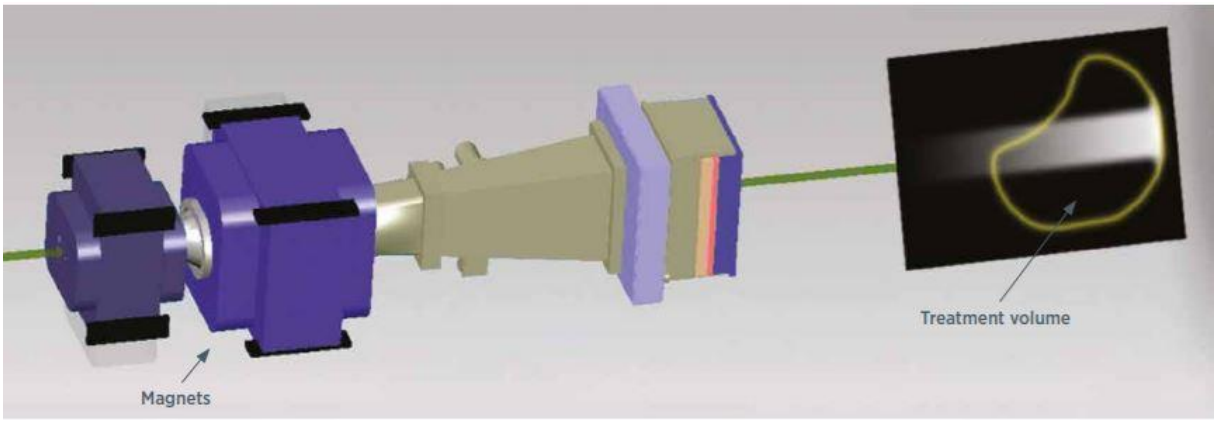

Figure 3: Proton Scanning diagram. [11]

1.3. The Current Problem without Adjoint Flux

In reactor physics the Monte Carlo (MC) method (or other approximations, like the S_N method) has been well established for calculating effective multiplication factors or dose rates in shielding problems. The power of the MC method lies in the possibility to include various desired variables and to represent accurately any physical model for particle scattering, cross section and/or geometrical complexity. The desired variables for proton therapy are three spatial coordinates, energy, two directional variables and time.

MC methods are a broad class of computational algorithms that rely on repeated random sampling to obtain numerical results. Their essential idea is using randomness to solve problems that might be deterministic in principle. Due to the statistical nature of the MC methods, the outcome always includes a statistical uncertainty. This uncertainty is proportional to the square root of the number of samples. To reduce the uncertainty with a factor of a hundred, one has to expand the sample size by a factor ten thousand. This slow reduction of uncertainty causes exponential increase of computation time, which is the biggest disadvantage of the MC method. If one is interested in quantities averaged over small intervals of one or more variables, the MC method becomes more and more inefficient. For this kind of problems the adjoint MC method comes in handy. The adjoint method provides a completely different equation, the so called 'importance' equation, that is simulated by MC.[6]

1.4. Goal of this Thesis

Current clinical dose calculation codes generally rely on semi-empirical methods that are fast and work well for geometrically simple problems, but are less accurate for practical, geometrically complex problems. The best known method that can cope with these kind of physical and geometrical complexity is the Monte Carlo method [3]. However a disadvantage of the Monte Carlo method is that accurate calculations with reasonably low errors take a lot of computation time. To reduce computation time a different method is introduced known as the S_n method. While the S_N method reduces the computation time, it still takes much time to run in order to reduce the errors significantly. In this thesis, a new approach for dose calculations aimed for radiotherapy treatment planning is introduced, based on the adjoint S_N method. Only a 1D geometry is examined for simplicity. The proposed approach is more accurate and has the promise to be faster than the current methods.

The goal of this thesis is to theoretically derive and numerically determine the adjoint proton flux. With this adjoint proton flux one can perform dose calculations much quicker and cheaper, because one can calculate changes in the response, without calculating the change of the flux. To reach this goal, the available models and literature on proton transport and adjoint calculation are being studied thoroughly.
The process to reach the goal can be structured into four individual parts. In section 2.1, the adjoint proton transport equation will be derived using the S_N method with the Fokker-Planck approximation. The S_N method with the Fokker-Planck approximation is validated in previous research reports.[14] In section 2.2 we derive an expression for response calculation with the help of adjoint theory. In section 2.3 of the thesis, an expression for the adjoint source is determined. There is an adjoint source expressed for one point and another expression for a certain tumour region. The adjoint source for a certain tumour region is eventually used for the numerical calculation of the adjoint proton flux. In section 3 the adjoint proton transport equation and the adjoint source are discretized, by inspecting the behaviour of the functions on the group boundaries and making use of linearity of flux and stopping power. In section 4, the numerical approach is worked out and tested. The result of this numerical calculation is provided and compared with a proven precise result. Due to this comparison one can check if the result makes sense and if it is practically applicable. Conclusions and recommendations for future work are made in section 5, regarding investigations which need to be performed in order to implement the adjoint proton flux in proton therapy practice.

This thesis is part of a bachelor research of Technology University of Delft at the section of Medical Physics and Technology at the Reactor Institute Delft.

2. Adjoint Calculations

In this chapter the adjoint proton transport equation will be derived. This derivation is based on a convenient additivity property of the adjoint. The adjoints of all the individual operators will be calculated separately and combined into one adjoint proton transport equation.
The adjoint source will be calculated in a similar way, with the help of perturbation theory calculations.

2.1. Calculation of the Adjoint Transport Equation

The transport equation for protons is derived from the linear 1D Boltzmann equation:

$$\hat{\Omega}\cdot\nabla\varphi(x,E,\hat{\Omega})+\sigma_t\varphi(x,E,\hat{\Omega})=\int_{4\pi}\int_{0}^{\infty}\sigma_s(x,E'\rightarrow E,\hat{\Omega}'\rightarrow\hat{\Omega})\,\varphi(x,E',\hat{\Omega}')dE'd\hat{\Omega}', \quad (2.1.1)$$

where φ(x,E,Ω), the angular proton flux, is the quantity considered in this equation. It is a particle density with kinetic energy E, moving in direction Ω through the surface at the point x. The first term of equation 2.1.1 is the streaming term, which describes the free movement of the particles through the domain. The second term of the left hand side of equation 2.1.1 is the total removal term, this term describes all interactions of particles that scatter to an energy different than E and another direction than Ω. The right hand side of equation 2.1.1 indicates the Boltzmann scatter operator. This operator describes all the particles that had initial energy E' and direction of movement Ω' and end up at the energy E and direction of movement Ω. [2]

After applying the Fokker-Planck Approximation and neglecting relatively small/unimportant terms we gain the 1D proton transport equation:

$$\mu\frac{\partial\varphi(x,E,\hat{\Omega})}{\partial x}+\sigma_t\varphi(x,E,\hat{\Omega})=\frac{\partial\left(S(E)\varphi(x,E,\hat{\Omega})\right)}{\partial E}+\frac{\sigma_{tr}}{2}\nabla_{\Omega}^{2}\varphi(x,E,\hat{\Omega}), \quad (2.1.2)$$

where μ is the cosine scatter angle, φ is the proton flux still depending on the position, kinetic energy and direction of movement, S(E) is the stopping power, σ_t is the total scatter cross section and σ_{tr} is a material based constant dependent of the differential cross section.
The first part of the left hand side of equation 2.1.2 still represents the streaming term. The second part of the left hand side of equation 2.1.2 is the total removal term. The second term of the right hand side of equation 2.1.2 is the continuous scatter operator and the first term of the right hand side is the continuous slowing down term. This term describes inelastic scatter whereupon little energy is lost in every collision [14].

The goal is to calculate the adjoint of the proton transport equation. The definition of the adjoint is:

$$< A\varphi, \varphi^{\dagger} > = < \varphi, A^{\dagger}\varphi^{\dagger} >, \tag{2.1.3}$$

where the brackets represent the inner product or the so called dot product. To calculate the adjoint of the transport equation one can use the fact that all the terms are linear. One property of the adjoint is that the adjoint of two linear terms equals the sum of the adjoint of the two individual parts.

$$(A_1 + A_2)^{\dagger} = {A_1}^{\dagger} + {A_2}^{\dagger} \tag{2.1.4}$$

Applying the additivity property from equation 2.1.4 on the proton transport equation results in:

$$A_1 + A_2 = A_3 + A_4 \rightarrow A_1^{\dagger} + A_2^{\dagger} = A_3^{\dagger} + A_4^{\dagger}, \tag{2.1.5}$$

where A_1-A_4 stand for the four individual operators of equation 2.1.2, later clarified in more detail.
So to calculate the adjoint transport equation, one can calculate the individual adjoint parts and assemble them together at the end.
We begin with the first part of equation 2.1.2 and define the corresponding operator:

$$A_1\varphi = \mu \frac{\partial \varphi(x, E, \hat{\Omega})}{\partial x} \rightarrow A_1 = \mu \frac{\partial}{\partial x}. \tag{2.1.6}$$

To determine the adjoint of this operator equation 2.1.7 needed to be solved:

$$< A_1\varphi, \varphi^{\dagger} > = \int_0^{\infty} dE \int_{4\pi} d\hat{\Omega} \int_0^{L} \mu \left(\frac{\partial}{\partial x}\varphi\right) \varphi^{\dagger} dx = < \varphi, A_1^{\dagger}\varphi^{\dagger} >. \tag{2.1.7}$$

The right-hand side of equation 2.1.7 can be integrated by parts to give:

$$\int_0^{\infty} dE \int_{4\pi} d\hat{\Omega} \left([\mu\varphi\varphi^{\dagger}]_0^L - \int_0^{L} \varphi \left(\mu \frac{\partial \varphi^{\dagger}}{\partial x}\right) dx \right). \tag{2.1.8}$$

To make the boundary term disappear, the boundary conditions have to be chosen such that:

$$[\mu\varphi\varphi^{\dagger}]_0^L = 0.$$

This relation holds because of the chosen boundary conditions:

$$\varphi(x=0,\mu>0)=0,\varphi(x=L,\mu<0)=0,\varphi^{\dagger}(x=0,\mu<0)=0,\varphi^{\dagger}(x=L,\mu>0)=0$$

Using $[\mu\varphi\varphi^{\dagger}]_0^L=0$ yields:

$$\int_0^{\infty} dE \int_{4\pi} d\hat{\Omega}\left(-\int_0^L \varphi\left(\mu\frac{\partial\varphi^{\dagger}}{\partial x}\right)dx\right)=<\varphi,A_1^{\dagger}\varphi^{\dagger}>. \tag{2.1.9}$$

$$A_1^{\dagger}=-A_1=-\mu\frac{\partial}{\partial x} \tag{2.1.10}$$

Take the second part of the Boltzmann proton transport equation (equation 2.1.2) and call this term A_2:

$$A_2\varphi=\sigma_t\varphi\left(x,E,\hat{\Omega}\right)\rightarrow A_2=\sigma_t. \tag{2.1.11}$$

Then a calculation of the inner product is performed:

$$<A_2\varphi,\varphi^{\dagger}>=\int_0^{\infty}\int_{4\pi}\int_0^L(\sigma_t\varphi)\varphi^{\dagger}dxd\hat{\Omega}dE=<\varphi,A_2^{\dagger}\varphi^{\dagger}>. \tag{2.1.12}$$

Inside the integral one may swap the order of terms to structure. So one can simply swap the order of the two phi's to determine the adjoint of this operator:

$$=\int_0^{\infty}\int_{4\pi}\int_0^L\varphi(\sigma_t\varphi^{\dagger})dxd\hat{\Omega}dE=<\varphi,A_2^{\dagger}\varphi^{\dagger}>. \tag{2.1.13}$$

From this calculation one can conclude the following:

$$A_2^{\dagger}=A_2=\sigma_t. \tag{2.1.14}$$

Taking the third part of the proton transport equation (equation 2.1.2) and defining its operator:

$$A_3\varphi = \frac{\partial\big(S(E)\varphi(x,E,\hat{\Omega})\big)}{\partial E} \rightarrow A_3 = \frac{\partial}{\partial E}(S(E)(.)). \tag{2.1.15}$$

To calculate the adjoint of the operator, equation 2.1.16 needed to be solved:

$$< A_3\varphi, \varphi^\dagger > = \int_0^L dx \int_{4\pi} d\hat{\Omega} \int_0^\infty \left(\frac{\partial}{\partial E}(S\varphi)\right)\varphi^\dagger dE =< \varphi, A_3^\dagger\varphi^\dagger >. \tag{2.1.16}$$

Integrating the right-hand side of 2.1.16 by parts results in:

$$\int_0^L dx \int_{4\pi} d\hat{\Omega}\left([\varphi^\dagger S\varphi]_0^\infty - \int_0^\infty S\varphi\frac{\partial}{\partial E}(\varphi^\dagger)dE\right). \tag{2.1.17}$$

To make the boundary term disappear, the boundary could have to be chosen properly:

$$\varphi(E=\infty) = 0, \varphi^\dagger(E=0) = 0.$$

So the boundary term disappears:

$$[\varphi^\dagger S\varphi]_0^\infty = 0$$

From the part that is left over from equation 2.1.17, we can determine the adjoint:

$$\int_0^L dx \int_{4\pi} d\hat{\Omega}\left(-\int_0^\infty S\varphi\frac{\partial}{\partial E}(\varphi^\dagger)dE\right) = < \varphi, A_3^\dagger\varphi^\dagger >. \tag{2.1.18}$$

$$A_3^\dagger = -S(E)\frac{\partial}{\partial E} \tag{2.1.19}$$

Taking the fourth and last part of equation 2.1.2 and once again defining the corresponding operator leads to:

$$A_4\varphi = \frac{\sigma_{tr}}{2}\nabla_\Omega^2\varphi\left(x, E, \widehat{\Omega}\right) \rightarrow A_4 = \frac{\sigma_{tr}}{2}\nabla_\Omega^2. \tag{2.1.20}$$

Once again, a calculation of the inner product is needed to determine the adjoint:

$$< A_4\varphi, \varphi^\dagger > = \int_0^L dx \int_0^\infty dE \int_{4\pi} \left(\frac{\sigma_{tr}}{2}\nabla_\Omega^2\varphi\right)\varphi^\dagger \, d\widehat{\Omega} =< \varphi, A_4^\dagger\varphi^\dagger >. \tag{2.1.21}$$

When integrating equation 2.1.21 by parts, one will get the following result:

$$= \int_0^L dx \int_0^\infty dE \left(\frac{\sigma_{tr}}{2}\left[\varphi^\dagger\nabla_\Omega\varphi\right]_{4\pi} - \frac{\sigma_{tr}}{2}\int_{4\pi} \nabla_\Omega \, \varphi^\dagger\nabla_\Omega\varphi d\widehat{\Omega}\right). \tag{2.1.22}$$

Due to Stokes' theorem, that says that a closed sphere has no boundary, the boundary terms will disappear. If the surface is closed one can use the divergence theorem. The divergence of the curl of a flux is zero. Intuitively if the total flux of the curl of a vector field over a surface is the work done against the field along the boundary of the surface then the total flux must be zero if the boundary is empty.

$$\left[\varphi^\dagger\nabla_\Omega\varphi\right]_{4\pi} = 0$$

When the boundary term disappears, one will end up with the following expression derived from equation 2.1.22:

$$\int_0^L dx \int_0^\infty dE \left(-\frac{\sigma_{tr}}{2}\int_{4\pi} \nabla_\Omega \, \varphi^\dagger\nabla_\Omega\varphi d\widehat{\Omega}\right). \tag{2.1.23}$$

Equation 2.1.23 needs to be integrated by parts once again, resulting in:

$$\int_0^L dx \int_0^\infty dE \left(-\frac{\sigma_{tr}}{2}\left[\nabla_\Omega\varphi^\dagger\varphi\right]_{4\pi} + \frac{\sigma_{tr}}{2}\int_{4\pi} \nabla_\Omega^2 \, \varphi^\dagger\varphi d\widehat{\Omega}\right). \tag{2.1.24}$$

$$-\left[\nabla_\Omega\varphi^\dagger\varphi\right]_{4\pi} = 0$$

(This holds again, because a closed sphere has no boundary.)

The result one ends up with is the following:

$$\int_0^L dx \int_0^\infty dE \left(+ \frac{\sigma_{tr}}{2} \int_{4\pi} \nabla_\Omega^2 \, \varphi^\dagger \varphi d\widehat{\Omega} \right) = < \varphi, A_4^\dagger \varphi^\dagger >. \tag{2.1.25}$$

$$A_4^\dagger = A_4 = \frac{\sigma_{tr}}{2} \nabla_\Omega^2 \tag{2.1.26}$$

When summing equation 2.1.10, 2.1.14 up on the left hand side of equation 2.1.27 and summing 2.1.19 and 2.1.26 up at the right hand side of equation 2.1.27, one will end up with the adjoint 1D proton transport equation:

$$-\mu \frac{\partial \varphi^\dagger(x, E, \widehat{\Omega})}{\partial x} + \sigma_t \varphi^\dagger(x, E, \widehat{\Omega}) = -S(E) \frac{\partial \varphi^\dagger \, (x, E, \widehat{\Omega})}{\partial E} + \frac{\sigma_{tr}}{2} \nabla_\Omega^2 \varphi^\dagger(x, E, \widehat{\Omega}). \tag{2.1.27}$$

2.2. Calculation of the Response Change

Perturbation theory and adjoint-based techniques can be very useful in certain types of transport calculations to solve complex models. In this specific case one uses perturbation theory to write down an expression for the change in response. Time-independent 1D fixed source calculations involve solving an inhomogeneous equation of the form:

$$B\varphi\left(x,E,\widehat{\Omega}\right)=S\left(x,E,\widehat{\Omega}\right), \tag{2.2.1}$$

where B corresponds to the linear Boltzmann equation, φ is the proton flux depending on depth, energy and direction. S is the fixed source of protons, which is considered to be an input quantity of this calculation.

The response a linear function:

$$R=<\Sigma_D,\varphi>, \tag{2.2.2}$$

where the brackets are indicating the 'dot product'. Calculating this dot product can be done by taking the integral over space, energy and direction and Σ_D is the response function.

Introducing a perturbed state as:

$$B\varphi'\left(x,E,\widehat{\Omega}\right)=S'\left(x,E,\widehat{\Omega}\right), \tag{2.2.3}$$

the corresponding response function is:

$$R'=<\Sigma_D,\varphi'>. \tag{2.2.4}$$

We define the adjoint equation for this problem by the following equation:

$$B^{\dagger}\varphi^{\dagger}\left(x,E,\widehat{\Omega}\right)=S^{\dagger}\left(x,E,\widehat{\Omega}\right). \tag{2.2.5}$$

By taking the dot product of equation 2.2.1 with the adjoint flux $\varphi^{\dagger}$ and taking the dot product of equation 2.2.5 with the flux φ, one ends up with equations 2.2.6 and 2.2.7:

$$<\varphi^{\dagger},B\varphi>=<\varphi^{\dagger},S> \tag{2.2.6}$$

$$<B^{\dagger}\varphi^{\dagger},\varphi>=<S^{\dagger},\varphi> \tag{2.2.7}$$

When subtracting equation 2.2.6 from equation 2.2.7 the following relation will come out:

$$< \varphi^{\dagger}, S > = < S^{\dagger}, \varphi > = R. \tag{2.2.8}$$

When following the same procedure for the perturbed response one finds:

$$< \varphi^{\dagger}, S' > = < S^{\dagger}, \varphi' > = R'. \tag{2.2.9}$$

Comparing equation 2.2.2 with equation 2.2.8 it turns out convenient to choose $S^{\dagger}$ as follows:

$$S^{\dagger} = \Sigma_D. \tag{2.2.10}$$

Subtracting equation 2.2.8 and equation 2.2.9 results in:

$$\Delta R = < \varphi^{\dagger}, (S' - S) > = < \varphi^{\dagger}, \Delta S >. \tag{2.2.11}$$

Perturbation theory can also be used to assess the effects of changing data appearing in the Boltzmann operator. Suppose that a perturbation is made in the cross section in the Boltzmann operator, then there will be a perturbation in the flux which will change the value computed for the change in the flux. The perturbed flux will obey the equation:

$$(B + \Delta B)(\varphi + \Delta\varphi) = S. \tag{2.2.12}$$

After simplifying equation 2.2.12 and neglecting the second-order term, the following relation is obtained for the change in the flux:

$$B\Delta\varphi \cong -\Delta B\varphi \tag{2.2.13}$$

Subtracting the inner product of $\varphi^{\dagger}$ with equation 2.2.13 and the inner product of $\Delta\varphi$ with equation 2.2.5 results in the following relation:

$$-< \varphi^{\dagger}, \Delta B\varphi > = < \Delta\varphi, S^{\dagger} > = < \Delta\varphi, \Sigma_D > = \Delta R \tag{2.2.14}$$

So one can now calculate the change in response by calculating ΔB, without calculating the change in flux (which costs a lot of time).

2.3. Calculation of the Adjoint Source

To determine the adjoint source one first needs to introduce the distribution of the deposited energy, making use of the energy flux:

$$\Phi^E(x) = \int_{E_{min}}^{E_{max}} \int_{4\pi} E\varphi(x, E, \hat{\Omega}) d\hat{\Omega} dE. \tag{2.3.1}$$

The energy flux is the amount of energy going through the point x in the domain and is used to obtain a balance equation of energy in a cell.
Multiplication of the 1D proton transport equation (equation 2.1.2) by the energy E, and integrating the result over the angular and energy domain results in the balance equation of energy in that cell. After filling in equation 2.1.2 into equation 2.3.1 we end up with the following expression:

$$\begin{aligned} &\int_{E_{min}}^{E_{max}} \int_{4\pi} E\mu \frac{\partial\varphi(x, E, \hat{\Omega})}{\partial x} d\hat{\Omega}\, dE + \int_{E_{min}}^{E_{max}} \int_{4\pi} E\sigma_t \varphi(x, E, \hat{\Omega}) d\hat{\Omega}\, dE \\ &= \int_{E_{min}}^{E_{max}} \int_{4\pi} E \frac{\partial(S(E)\varphi(x, E, \hat{\Omega}))}{\partial E} d\hat{\Omega} dE + \int_{E_{min}}^{E_{max}} \int_{4\pi} E \frac{\sigma_{tr}}{2} \nabla_{\hat{\Omega}}^2 \varphi(x, E, \hat{\Omega}) d\hat{\Omega} dE. \end{aligned} \tag{2.3.2}$$

$\int_{E_{min}}^{E_{max}} \int_{4\pi} E \frac{\sigma_{tr}}{2} \nabla_{\hat{\Omega}}^2 \varphi(x, E, \hat{\Omega}) d\hat{\Omega} dE$ is zero in this scenario, since no energy is created in this process. And therefore this term does not have any impact on the deposited energy balance equation.
The first term on the left hand side is a streaming term and represents the nett energy flow through the domain. This term is not a deposition term. The second term on the left hand side is a deposition term. This term represents the total amount of energy which has been removed due to scatter interactions. For simplicity we neglect this term in further calculations.
Therefore the stopping power term is the only deposition term to take into account:

$$\int_{E_{min}}^{E_{max}} \int_{4\pi} E \frac{\partial(S(E)\varphi(x, E))}{\partial E} d\hat{\Omega}\, dE. \tag{2.3.3}$$

We change the order of integration for simplicity:

$$\int_{4\pi} d\hat{\Omega} \int_{E_{min}}^{E_{max}} E \frac{\partial(S(E)\varphi(x, E))}{\partial E} dE. \tag{2.3.4}$$

And apply integration by parts to find an expression for the deposited energy:

$$\int_{4\pi} d\hat{\Omega} \left([S(E)\varphi(x,E)E]_{E_{min}}^{E_{max}} - \int_{E_{min}}^{E_{max}} S(E)\varphi(x,E)dE \right). \tag{2.3.5}$$

We choose the boundary condition to be:

$$\varphi(x, E = E_{max}) = 0.$$

And therefore this is the result of equation 2.3.6, after applying boundary conditions:

$$-\int_{4\pi} d\hat{\Omega} \left(S(E_{min})\varphi(x,E_{min})E_{min} + \int_{E_{min}}^{E_{max}} S(E)\varphi(x,E)dE \right). \tag{2.3.6}$$

The goal of this calculation is to determine the gain of protons. The integral over the transport equation gives the loss of protons. To give the response of the system one need to simply multiply the result from equation 2.3.6 with -1:

$$\int_{4\pi} d\hat{\Omega} \left(S(E_{min})\varphi(x,E_{min})E_{min} + \int_{E_{min}}^{E_{max}} S(E)\varphi(x,E)dE \right). \tag{2.3.7}$$

A calculation of the system's response by integrating equation 2.3.7 over x is done:

$$R = \int_0^L \int_{4\pi} d\hat{\Omega} \left(\left(S(E_{min})\varphi(x,E_{min})E_{min} + \int_{E_{min}}^{E_{max}} S(E)\varphi(x,E)dE \right) \cdot f(x) \right) dx. \tag{2.3.8}$$

Defining f(x) as a response over a certain region (1) (tumour length) and defining f(x) as a response at a certain point x_0 (2).

$$\begin{aligned} f(x) &= u(x_{min}) - u(x_{max}) \quad (1) \\ f(x) &= \delta(x - x_0) \quad (2) \end{aligned} \tag{2.3.9}$$

u(x) is the unit step function $u(x) = \begin{cases} 0, & x < 0 \\ 1, & x \geq 0 \end{cases}$ and with $\delta(x-x_0)$ a Delta-Dirac function at $x=x_0$.

The calculation of the response over the region using expression (1) of f(x) is done first:

$$R = \int_{4\pi} d\hat{\Omega} \int_{x_{min}}^{x_{max}} \left(S(E_{min})\varphi(x, E_{min})E_{min} + \int_{E_{min}}^{E_{max}} S(E)\varphi(x, E)dE \right). \tag{2.3.10}$$

It turns out to be clever to write the response as an integral over depth, energy and direction so that one can directly write down $S^{\dagger}$, according to the definition of $S^{\dagger}$ formulated in equation 2.2.8.

$$\begin{aligned} R = &\int_{4\pi} d\hat{\Omega} \int_{0}^{L} \int_{E_{min}}^{E_{max}} S(E)\varphi(x, E)E\delta(E - E_{min})\big(u(\mathrm{x}_{min}) - u(x_{max})\big)\, dE\, dx \\ &+ \int_{4\pi} d\hat{\Omega} \int_{0}^{L} \int_{E_{min}}^{E_{max}} S(E)\varphi(x, E)\big(u(\mathrm{x}_{min}) - u(x_{max})\big)dEdx. \end{aligned} \tag{2.3.11}$$

So the adjoint source over a tumour region equals:

$$S^{\dagger} = \Sigma_D = S(E)\big(u(\mathrm{x}_{min}) - u(x_{max})\big)\big(1 + E\delta(E - E_{min})\big). \tag{2.3.12}$$

To determine the adjoint source for a point one has to repeat the same calculations as equation 2.3.10 and equation 2.3.11 for $f(x)=\delta(x-x_0)$

$$R = \int_{4\pi} d\hat{\Omega} \int_{0}^{L} \left(S(E_{min})\varphi(x, E_{min})E_{min}\delta(x - x_0) + \int_{E_{min}}^{E_{max}} S(E)\varphi(x, E)\delta(x - x_0)dE \right). \tag{2.3.13}$$

$$\begin{aligned} R = &\int_{4\pi} d\hat{\Omega} \int_{0}^{L} \int_{E_{min}}^{E_{max}} S(E)\varphi(x, E)E\delta(E - E_{min})\delta(x - x_0)\, dE\, dx + \\ &\int_{4\pi} d\hat{\Omega} \int_{0}^{L} \int_{E_{min}}^{E_{max}} S(E)\varphi(x, E)\delta(x - x_0)dEdx. \end{aligned} \tag{2.3.14}$$

Ending up with the adjoint source for a point:

$$S^{\dagger} = \Sigma_D = S(E)\delta(x - x_0)(1 + E\delta(E - E_{min})). \tag{2.3.15}$$

2.4. Conclusions

The Boltzmann Fokker-Planck approximation is introduced to describe the transport of protons. This approximation consists of four terms: streaming, total removal, continuous slowing down and continuous scatter. With this approximation one calculated the adjoint proton transport equation, making use of additivity of the individual terms and smart choices of boundary conditions.

An expression for response changes is derived. The change in response can be calculated without having to calculate the changes in the Boltzmann Fokker-Planck approximation, but with the help of the adjoint.

The systems' response is calculated. Therefore we first determined the deposited energy terms and added a test function to provide response in a certain tumour region and/or response for a single point inside the body.

3. Discretization

With the adjoint proton transport equation and adjoint source one can determinate the adjoint proton flux. This determination has to be done numerically. To code this down, one needs to discretize the adjoint continuous slowing down operator and the adjoint proton source. The general procedure in discretizing an independent variable is to divide the range of the variable into a number of cells and subsequently integrate the transport equation over the volume of each cell. A coupled set of equations, describing the flux inside the cell is the result.
These terms both include the stopping power which is assumed to be linear inside a cell.

3.1. Discretization of the Adjoint Continuous Slowing Down Operator

The discretization of the energy variable is the so called multi-group method. The energy range is divided into a number of cells which are called energy groups. The energy group with the highest energy corresponds to g=1. For the energy domain, we use the linear discontinuous Galerkin method. This method is assuming a linear flux inside one energy group and can be discontinuous at the boundaries of each energy group.

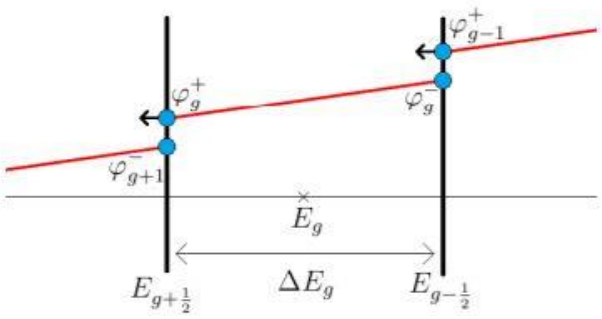

Figure 4: Representation of the Galerkin method used to discretize the adjoint slowing down and adjoint source terms. [5],[14]

As calculated in equation 2.1.19 the adjoint operator of the stopping power term equals:

$$L^{\dagger}_{CSD} = -S(E)\frac{\partial}{\partial E} \tag{3.1.1}$$

To determine the proton flux inside each energy group it is smart move to express this flux in another way using this set of (orthogonal) basis functions:

$$\begin{aligned} p^A(E) &= p^0(E) = 1 \\ p^E(E) &= p^1(E) = \frac{2}{\Delta E_g}\left(E - E_g\right), \end{aligned} \tag{3.1.2}$$

where ΔE_g stands for the width of the g^{th} energy group. And E_g is the centre energy value of energy group g.

Due to the orthogonality of the basis functions, the following orthogonality property holds:

$$\int_{E_{g+\frac{1}{2}}}^{E_{g-\frac{1}{2}}} p^i(E)p^j(E)dE = \frac{\Delta E_g}{2j+1}\delta_{ij}. \tag{3.1.3}$$

The proton flux expressed in the basis functions will look like this:

$$\varphi^{\dagger}_{i,n,g} = \varphi^{\dagger}_{a,i,n,g}(E)p^A(E) + \varphi^{\dagger}_{e,i,n,g}(E)p^E(E). \tag{3.1.4}$$

$\varphi_{a,i,n,g}$ is the average adjoint flux in spatial cell *i*, discrete ordinate *n* and energy group *g*. $\varphi_{e,i,n,g}$ is the normalized slope of the adjoint flux in spatial cell *i*, discrete ordinate *n* and energy group *g*.

It is also possible to express the stopping power with the same set of basis functions as the flux in the energy groups:

$$S(E) = \frac{S_{g+\frac{1}{2}} + S_{g-\frac{1}{2}}}{2}p^A(E) + \frac{S_{g-\frac{1}{2}} - S_{g+\frac{1}{2}}}{2}p^E(E). \tag{3.1.5}$$

Since there are two unknowns per energy group, the average flux and the slope of the flux, one needs two equations in each group to solve these unknowns. To obtain these equations an expansion of the flux into the two basis functions, multiply the equation by one of the basis functions, integrate over the volume of an energy group and use the upwind scheme to evaluate the surface integrals is needed.

To determine the average part of the equation, equation 3.1.6 has to be solved:

$$\frac{1}{\Delta E_g}\int_{E_{g+\frac{1}{2}}}^{E_{g-\frac{1}{2}}} L^{\dagger}_{CSD}\,\varphi^{\dagger}_{i,n,g}(E)p^A(E)dE, \tag{3.1.6}$$

which equals:

$$= \frac{1}{\Delta E_g}\int_{E_{g+\frac{1}{2}}}^{E_{g-\frac{1}{2}}} -S(E)\frac{\partial}{\partial E}\left(\varphi^{\dagger}_{i,n,g}(E)\right)p^A(E)dE. \tag{3.1.7}$$

Integrating by parts and making use of the fact that $p^A(E)$ equals 1 result in:

$$\frac{1}{\Delta E_g}\int_{E_{g+\frac{1}{2}}}^{E_{g-\frac{1}{2}}}\frac{\partial}{\partial E}\big(S(E)\big)\varphi^{\dagger}_{i,n,g}(E)p^A(E)dE-\frac{1}{\Delta E_g}\Big[S(E)\varphi^{\dagger}_{i,n,g}(E)\Big]_{E_{g+\frac{1}{2}}}^{E_{g-\frac{1}{2}}} \tag{3.1.8}$$

When evaluating the surface integral using the upwind scheme this is the result:

$$\begin{aligned}&\int_{E_{g+\frac{1}{2}}}^{E_{g-\frac{1}{2}}} L^{\dagger}_{CSD}\,\varphi^{\dagger}_{i,n,g}(E)p^A(E)dE=\\&\frac{1}{\Delta E_g}\int_{E_{g+\frac{1}{2}}}^{E_{g-\frac{1}{2}}}\frac{\partial}{\partial E}\big(S(E)\big)\varphi^{\dagger}_{i,n,g}(E)p^A(E)dE\\&-\frac{1}{\Delta E_g}\Big(S_{g-\frac{1}{2}}(\varphi^{\dagger}_{a,i,n,g}+\varphi^{\dagger}_{e,i,n,g})-S_{g+\frac{1}{2}}(\varphi^{\dagger}_{a,i,n,g+1}+\varphi^{\dagger}_{e,i,n,g+1})\Big).\end{aligned} \tag{3.1.9}$$

The first part of the right-hand side of equation 3.1.9 can be worked out even further:

$$\frac{1}{\Delta E_g}\int_{E_{g+\frac{1}{2}}}^{E_{g-\frac{1}{2}}}\frac{\partial}{\partial E}\big(S(E)\big)\varphi^{\dagger}_{i,n,g}(E)p^A(E)dE=\frac{1}{\Delta E_g}\int_{E_{g+\frac{1}{2}}}^{E_{g-\frac{1}{2}}}\frac{\left(S_{g-\frac{1}{2}}-S_{g+\frac{1}{2}}\right)}{\Delta E_g}\varphi^{\dagger}_{i,n,g}(E)p^A(E)dE. \tag{3.1.10}$$

When we work out the integral in the right hand side of equation 3.1.10 by making use of the orthogonality property in equation (3.1.3) we end up with equation 3.1.11:

$$\frac{\left(S_{g-\frac{1}{2}}-S_{g+\frac{1}{2}}\right)}{\Delta E_g}\varphi^{\dagger}_{a,i,n,g}. \tag{3.1.11}$$

Substituting the integral in equation 3.1.9 with the result of equation 3.1.11 results in:

$$\int_{E_{g+\frac{1}{2}}}^{E_{g-\frac{1}{2}}} L_{CSD}^{\dagger}\,\varphi_{i,n,g}^{\dagger}(E)p^{A}(E)dE = \frac{\left(S_{g-\frac{1}{2}}-S_{g+\frac{1}{2}}\right)}{\Delta E_g}\varphi_{a,i,n,g}^{\dagger} - \frac{1}{\Delta E_g}\left(S_{g-\frac{1}{2}}\left(\varphi_{a,i,n,g}^{\dagger}+\varphi_{e,i,n,g}^{\dagger}\right) - S_{g+\frac{1}{2}}\left(\varphi_{a,i,n,g+1}^{\dagger}+\varphi_{e,i,n,g+1}^{\dagger}\right)\right), \tag{3.1.12}$$

where $\frac{\left(S_{g-\frac{1}{2}}-S_{g+\frac{1}{2}}\right)}{\Delta E_g}\varphi_{a,i,n,g}^{\dagger}$ is the volumetric term, $-\frac{1}{\Delta E_g}S_{g-\frac{1}{2}}\left(\varphi_{a,i,n,g}^{\dagger}+\varphi_{e,i,n,g}^{\dagger}\right)$ is the group outflow and $\frac{1}{\Delta E_g}S_{g+\frac{1}{2}}\left(\varphi_{a,i,n,g+1}^{\dagger}+\varphi_{e,i,n,g+1}^{\dagger}\right)$ represents the flux flowing in.

For the slope part of the equation we multiply the continuous slowing down operator by $p^E(E)$ and integrate over an energy group:

$$\frac{3}{\Delta E_g}\int_{E_{g+\frac{1}{2}}}^{E_{g-\frac{1}{2}}} L_{CSD}^{\dagger}\varphi_{i,n,g}^{\dagger}(E)p^{E}(E)dE. \tag{3.1.13}$$

$$\frac{3}{\Delta E_g}\int_{E_{g+\frac{1}{2}}}^{E_{g-\frac{1}{2}}} -S(E)\left(\frac{\partial}{\partial E}\varphi_{i,n,g}^{\dagger}(E)\right)p^{E}(E)dE. \tag{3.1.14}$$

Making use of partial integration results in:

$$\frac{3}{\Delta E_g}\int_{E_{g+\frac{1}{2}}}^{E_{g-\frac{1}{2}}} \frac{\partial}{\partial E}\left(S(E)p^{E}(E)\right)\varphi_{i,n,g}^{\dagger}(E)dE - \frac{3}{\Delta E_g}\left[S(E)\varphi_{i,n,g}^{\dagger}(E)p^{E}(E)\right]_{E_{g+\frac{1}{2}}}^{E_{g-\frac{1}{2}}} \tag{3.1.15}$$

Here one uses the same upwind scheme as done at equation 3.1.9:

$$\int_{E_{g+\frac{1}{2}}}^{E_{g-\frac{1}{2}}} L_{CSD}^{\dagger}\varphi_{i,n,g}^{\dagger}(E)p^{E}(E)dE = \frac{3}{\Delta E_g}\int_{E_{g+\frac{1}{2}}}^{E_{g-\frac{1}{2}}} \frac{\partial}{\partial E}\left(S(E)p^{E}(E)\right)\varphi_{i,n,g}^{\dagger}(E)dE - \frac{3}{\Delta E_g}\left(S_{g-\frac{1}{2}}\left(\varphi_{a,i,n,g}^{\dagger}+\varphi_{e,i,n,g}^{\dagger}\right)p^{E}(E_{g-1/2}) - S_{g+\frac{1}{2}}\left(\varphi_{a,i,n,g+1}^{\dagger}+\varphi_{e,i,n,g+1}^{\dagger}\right)p^{E}(E_{g+1/2})\right). \tag{3.1.16}$$

The first term of the right-hand side of equation 3.1.16 can be worked that out even further:

$$\frac{3}{\Delta E_g}\int_{E_{g+\frac{1}{2}}}^{E_{g-\frac{1}{2}}}\frac{\partial}{\partial E}\left(S(E)p^E(E)\right)\varphi^{\dagger}_{i,n,g}(E)dE = \tag{3.1.17}$$

$$\frac{3}{\Delta E_g}\int_{E_{g+\frac{1}{2}}}^{E_{g-\frac{1}{2}}}\frac{\partial S(E)}{\partial E}p^E(E)\varphi^{\dagger}_{i,n,g}(E)dE + \frac{3}{\Delta E_g}\int_{E_{g+\frac{1}{2}}}^{E_{g-\frac{1}{2}}}S(E)\frac{\partial p^E(E)}{\partial E}\varphi^{\dagger}_{i,n,g}(E)dE =$$

$$\frac{1}{\Delta E_g}\left(S_{g-\frac{1}{2}}-S_{g+\frac{1}{2}}\right)\varphi^{\dagger}_{e,i,n,g}+\frac{3}{\Delta E_g}\left(S_{g+\frac{1}{2}}+S_{g-\frac{1}{2}}\right)\varphi^{\dagger}_{a,i,n,g}+\frac{1}{\Delta E_g}\left(S_{g-\frac{1}{2}}-S_{g+\frac{1}{2}}\right)\varphi^{\dagger}_{e,i,n,g} \tag{3.1.18}$$
$$=\frac{3}{\Delta E_g}\left(S_{g+\frac{1}{2}}+S_{g-\frac{1}{2}}\right)\varphi^{\dagger}_{a,i,n,g}+\frac{2}{\Delta E_g}\left(S_{g-\frac{1}{2}}-S_{g+\frac{1}{2}}\right)\varphi^{\dagger}_{e,i,n,g}$$

Making use of the fact that $p^E(E_{g-1/2}) = 1$ and $p^E(E_{g+1/2}) = -1$ and substituting the integral in equation 3.1.16 with the result of equation 3.1.18 results in:

$$\int_{E_{g+\frac{1}{2}}}^{E_{g-\frac{1}{2}}}L^{\dagger}_{CSD}\varphi^{\dagger}_{i,n,g}(E)p^E(E)dE = \frac{3}{\Delta E_g}\left(S_{g+\frac{1}{2}}+S_{g-\frac{1}{2}}\right)\varphi^{\dagger}_{a,i,n,g}+\frac{2}{\Delta E_g}\left(S_{g-\frac{1}{2}}-S_{g+\frac{1}{2}}\right)\varphi^{\dagger}_{e,i,n,g} \tag{3.1.19}$$
$$-\frac{3}{\Delta E_g}\left(S_{g-\frac{1}{2}}\left(\varphi^{\dagger}_{a,i,n,g}+\varphi^{\dagger}_{e,i,n,g}\right)+S_{g+\frac{1}{2}}\left(\varphi^{\dagger}_{a,i,n,g+1}+\varphi^{\dagger}_{e,i,n,g+1}\right)\right),$$

where $\frac{3}{\Delta E_g}\left(S_{g+\frac{1}{2}}+S_{g-\frac{1}{2}}\right)\varphi^{\dagger}_{a,i,n,g}+\frac{2}{\Delta E_g}\left(S_{g-\frac{1}{2}}-S_{g+\frac{1}{2}}\right)\varphi^{\dagger}_{e,i,n,g}$ are volumetric terms,
$-\frac{3}{\Delta E_g}S_{g-\frac{1}{2}}\left(\varphi^{\dagger}_{a,i,n,g}+\varphi^{\dagger}_{e,i,n,g}\right)$ is the flux flowing out of the group and
$-\frac{3}{\Delta E_g}S_{g+\frac{1}{2}}\left(\varphi^{\dagger}_{a,i,n,g+1}+\varphi^{\dagger}_{e,i,n,g+1}\right)$ is the flux flowing in the group.

3.2. Discretization of the Adjoint Source

As calculated in equation 2.3.12 the adjoint source for a tumour region/slab equals:

$$S^{\dagger} = S(E)(u(x_{min}) - u(x_{max}))(1 + E\delta(E - E_{min})) \tag{3.2.1}$$

To discretize this adjoint one can use the same approach as the discretization for the energy. The basis functions mentioned in the energy discretization part (equation 3.1.2) are the same for the adjoint source discretization.

To determine the average part of equation 3.2.1, equation 3.2.2 has to be solved:

$$\frac{1}{\Delta E_g}\int_{E_{g+\frac{1}{2}}}^{E_{g-\frac{1}{2}}} S(E)\,(u(x_{min}) - u(x_{max}))\big(1 + E\delta(E - E_{min})\big)p^A(E)dE \tag{3.2.2}$$

$$(u(x_{min}) - u(x_{max}))\left(\frac{1}{\Delta E_g}\int_{E_{g+\frac{1}{2}}}^{E_{g-\frac{1}{2}}} S(E)\,p^A(E)dE + \frac{1}{\Delta E_g}\int_{E_{g+\frac{1}{2}}}^{E_{g-\frac{1}{2}}} ES(E)\delta(E - E_{min})p^A(E)dE\right). \tag{3.2.3}$$

The $ES(E)\delta(E\text{-}E_{min})$ term in equation 3.2.3 equals zero except if the minimum energy is in between the two lowest energy boundaries.
The first integral in equation 3.2.3 can be worked out even further:

$$\frac{1}{\Delta E_g}\int_{E_{g+\frac{1}{2}}}^{E_{g-\frac{1}{2}}} S(E)p^A(E)\,dE = \tag{3.2.4}$$
$$\frac{1}{\Delta E_g}\int_{E_{g+\frac{1}{2}}}^{E_{g-\frac{1}{2}}}\left(\frac{S_{g+\frac{1}{2}} + S_{g-\frac{1}{2}}}{2}p^A(E) + \frac{S_{g-\frac{1}{2}} - S_{g+\frac{1}{2}}}{2}p^E(E)\right)p^A(E)dE.$$

Making use of the orthogonality of the basis functions in equation 3.1.3:

$$\frac{1}{\Delta E_g}\left(\frac{S_{g+\frac{1}{2}} + S_{g-\frac{1}{2}}}{2}\right)\Delta E_g = \left(\frac{S_{g+\frac{1}{2}} + S_{g-\frac{1}{2}}}{2}\right). \tag{3.2.5}$$

Finally ending up with this discretization for the average part of adjoint source:

$$\int_{E_{g+\frac{1}{2}}}^{E_{g-\frac{1}{2}}} S(E)\left(u(x_{min})-u(x_{max})\right)\left(1+E\delta(E-E_{min})\right)p^A(E)dE = \left(u(x_{min})-u(x_{max})\right)\left(\left(\frac{S_{g+\frac{1}{2}}+S_{g-\frac{1}{2}}}{2}\right)+\frac{1}{\Delta E_g}\int_{E_{g+\frac{1}{2}}}^{E_{g-\frac{1}{2}}} ES(E)\delta(E-E_{min})dE\right). \quad (3.2.6)$$

To determine the slope part of equation 3.2.1, equation 3.2.7 has to be solved:

$$\frac{3}{\Delta E_g}\int_{E_{g+\frac{1}{2}}}^{E_{g-\frac{1}{2}}} S(E)\left(u(x_{min})-u(x_{max})\right)\left(1+E\delta(E-E_{min})\right)p^E(E)dE = \quad (3.2.7)$$

$$\left(u(x_{min})-u(x_{max})\right)\left(\frac{3}{\Delta E_g}\int_{E_{g+\frac{1}{2}}}^{E_{g-\frac{1}{2}}} S(E)\,p^E(E)dE+\frac{3}{\Delta E_g}\int_{E_{g+\frac{1}{2}}}^{E_{g-\frac{1}{2}}} ES(E)\delta(E-E_{min})p^E(E)dE\right). \quad (3.2.8)$$

The last integral term in equation 3.2.8 equals zero except the case where the minimum energy is in between the groups with the lowest energy. The first integral in equation 3.2.8 can be worked out even further:

$$\frac{3}{\Delta E_g}\int_{E_{g+\frac{1}{2}}}^{E_{g-\frac{1}{2}}} S(E)\,p^E(E)dE = \frac{3}{\Delta E_g}\int_{E_{g+\frac{1}{2}}}^{E_{g-\frac{1}{2}}}\left(\frac{S_{g+\frac{1}{2}}+S_{g-\frac{1}{2}}}{2}p^A(E)+\frac{S_{g-\frac{1}{2}}-S_{g+\frac{1}{2}}}{2}p^E(E)\right)p^E(E)dE. \quad (3.2.9)$$

Making use of the orthogonality of the basis functions in equation 3.1.3:

$$\frac{3}{\Delta E_g}\cdot\frac{1}{3}\left(\frac{S_{g-\frac{1}{2}}-S_{g+\frac{1}{2}}}{2}\right)\Delta E_g = \left(\frac{S_{g-\frac{1}{2}}-S_{g+\frac{1}{2}}}{2}\right). \quad (3.2.10)$$

So this is the final expression for the slope part:

$$\left(u(x_{min})-u(x_{max})\right)\left(\left(\frac{S_{g-\frac{1}{2}}-S_{g+\frac{1}{2}}}{2}\right)+\frac{3}{\Delta E_g}\int_{E_{g+\frac{1}{2}}}^{E_{g-\frac{1}{2}}} ES(E)\delta(E-E_{min})p^E(E)dE\right). \quad (3.2.11)$$

3.3. Computational Set-up

A numerical code is created to calculate fluxes in forward mode and in adjoint mode. This code solves the 1D transport equation to obtain the average flux and the slope of the flux. In this code one can vary every single parameter that has influence on the flux. In this research we have only one spatial variable x, because we do calculations in 1D, and that is defined between 0 and 10 cm, that corresponds to the 1st and 128th element. We vary the energy of the incoming proton beam between 2MeV and 100MeV and divide that energy equally over the energy groups. The boundaries of those energy groups are specified in the following way:

$$E_{\frac{1}{2}} = E_{in} + \frac{1}{2}\Delta E \tag{3.3.1}$$

$$\Delta E = \frac{E_{max} - E_{min}}{Number\ of\ groups}. \tag{3.3.2}$$

To compare results and discretization we set the number of energy groups initially at 128 and compare it with 256 energy groups. In the numerical approach we have used 4 angular elements that correspond to the direction of movement. The total macroscopic scatter cross section and transport cross section are constants inside the code, with the transport cross section equal to 0. The tumour region can be adapted inside the code, but normally be between the 1st and 128th space element.

3.4. Conclusions

To implement the adjoint flux and adjoint source inside a numerical code, we first have to discretize the continuous slowing down term and the adjoint source. Therefore we transform the adjoint transport equation and the adjoint source into a set of coupled orthogonal basis functions. In this thesis we choose the linear discontinuous Galerkin discretization method, to discretize the terms. In order to discretize these terms, we assumed that the flux is linear inside an energy group and that the stopping power is linear as well.

4. Results

The discretized adjoint transport equation is a set of linear equations. As adjoint protons stream through the domain they gain energy, which is what the adjoint continuous slowing down operator describes. We'll give the protons an initial energy of 2 MeV, and the protons stream out of the system at the upper energy boundary of 100 MeV. These boundaries are proven to give be the best working range when using the S_N method.[14] When we increase energy, energy will be transferred to secondary particles, like electrons and neutrons, inside the body, which are not included in the S_N approximation. This energy which would have been carried by these particles is assumed to deposit locally. The two equations that describe the angular proton flux are calculated as follows:

$$\begin{bmatrix} m_{11} & m_{12} \\ m_{21} & m_{22} \end{bmatrix} * \begin{bmatrix} \varphi^{\dagger}_{a,i,n,g} \\ \varphi^{\dagger}_{e,i,n,g} \end{bmatrix} = \begin{bmatrix} a_1 \\ a_2 \end{bmatrix}. \tag{4.1}$$

The matrix $\begin{bmatrix} m_{11} & m_{12} \\ m_{21} & m_{22} \end{bmatrix}$ in equation 4.1 is filled with all variables that directly depend on the average and slope of the adjoint flux in the group that we try to solve. Variables that directly depend on these functions are outflow and volumetric terms. The array $\begin{bmatrix} a_1 \\ a_2 \end{bmatrix}$ in the right hand side of equation 4.1 is filled with volumetric source terms and terms that depend on neighbour groups like inflow from lower energy groups. These terms can be found in equation 3.1.12 for the average adjoint flux and in equation 3.1.19 for the slope adjoint flux.

The discretized terms derived in Section 3.2. and Section 3.3. are implemented into a numerical code that solves this set of equations simultaneously, since average adjoint flux and slope adjoint flux are coupled. In this research we used Fortran to solve this problem and try to find values for average adjoint flux and for slope adjoint flux in each energy group. Fortran is especially suited for numeric computation and scientific computing[9]. The terms that are implemented into the code are tested for two simple cases (see Appendix 1). The goal of the thesis is to calculate response changes due to input changes, with the adjoint proton flux. We choose the stopping power to be: $S(E) = \frac{1.88506*10^9}{3.5269*10^{-6}E+2}$. This expression for the stopping power isn't the true value of stopping power inside the body, but works well enough to conclude relevant meaningful results.

4.1. Adjoint Flux

At first we tried to plot the adjoint flux and try to validate and check if these plots make sense.

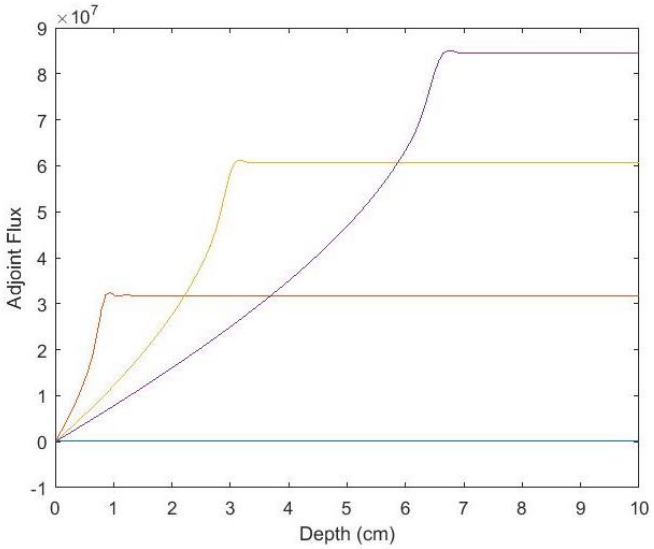

Figure 5: A plot of the adjoint flux for the 126th energy group (blue), 84th energy group (red), 42nd energy group (yellow) and first energy group (purple). Assuming the tumour/adjoint source is on the whole x-domain [0-10]. (Plot with the adjoint source on the whole space domain, 128 energy groups, 128 space elements and 1 angular element μ = -0.7092178.)

In the graph of figure 5 we see that adjoint protons stream from right to left and will gain energy while decreasing in group number. This means that the energy will flow from higher groups to lower groups. Particles in the lowest energy group will have the largest energy, due to energy gaining in the higher neighbour groups. Particles in the highest energy group will not gain energy because the instream of this group is set to zero in the numerical code.
To show the function of the angular element the following graph is plotted:

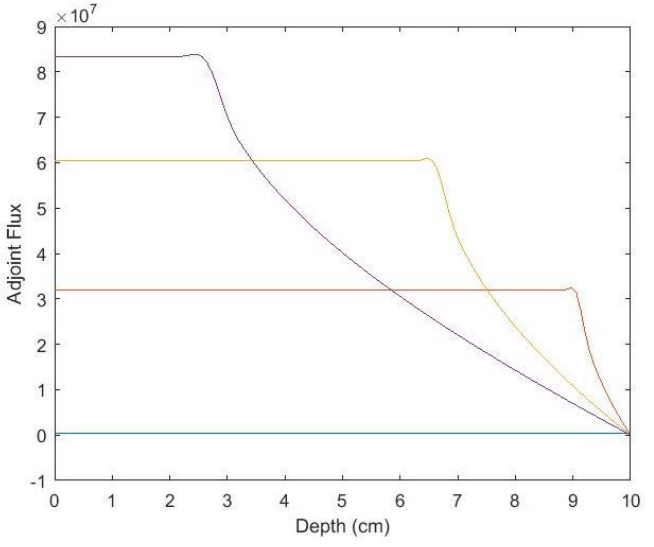

Figure 6: A plot of the adjoint flux for the 126th energy group (blue), 84th energy group (red), 42nd energy group (yellow) and first energy group (purple). Assuming the tumour/adjoint source is on the whole x-domain [0-10]. (Plot with the adjoint source on the whole space domain, 128 energy groups, 128 space elements and 1 angular element μ = +0.7880198.)

The graph shown in figure 6 is almost identical to the graph in figure 5, except the fact that particles will stream from left to right. Therefore we perceive this difference.

In practice the tumour is most of the time not on the whole domain of 0 to 10 cm and therefore we plotted a graph with a local tumour/adjoint source from element number 70 to 100, corresponding to a depth of 5.47cm to 7.81cm. This tumour location is not chosen randomly. We want to treat the tumour at the Bragg peak of the dose. The location of the Bragg peak can be determined by making a plot of the dose, as shown in figure 7. During treatment we want the Bragg peak to overlap with the tumour region and therefore we choose the tumour to be between the 70th and 100th space element (5.47cm-7.81cm).

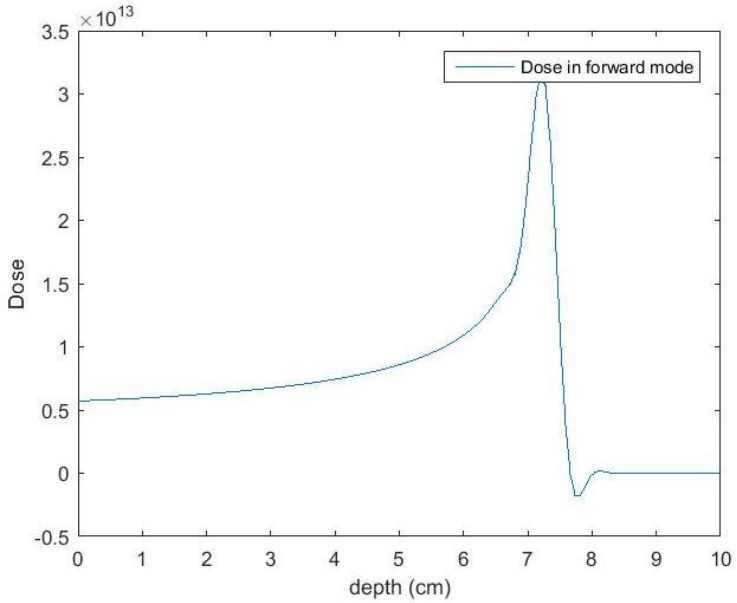

Figure 7: Plot of the dose distribution in forward calculations. (Plot details: 128 energy groups, 128 space elements and 1 angular element μ = -0.7092178.)

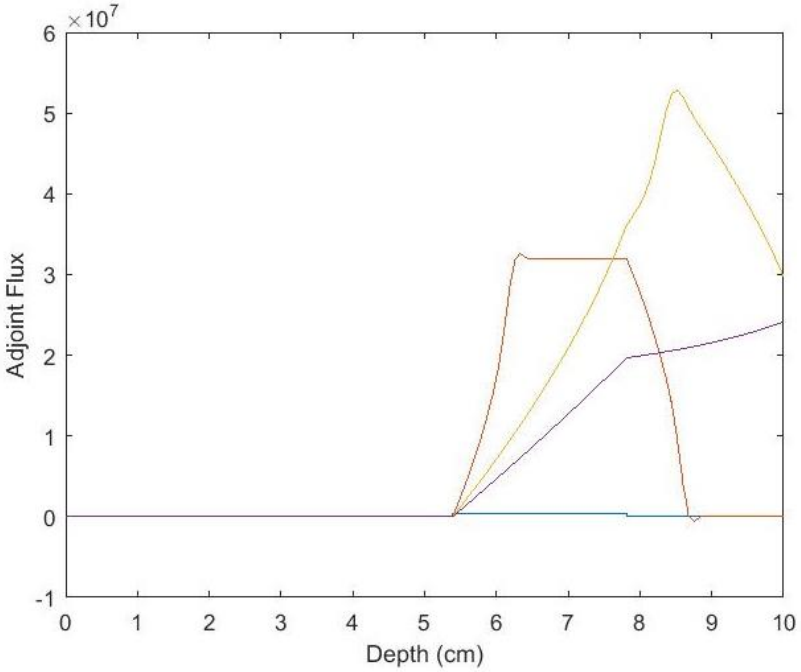

Figure 8: A plot of the adjoint flux for the 126th energy group (blue), 84th energy group (red), 42nd energy group (yellow) and first energy group (purple). Assuming the tumour/adjoint source is between the 70th and 100th element. (Plot with the adjoint source between the 70th and 100th space element (5.47cm-7.81cm), 128 energy groups, 128 space elements and 1 angular element μ = -0.7092178.)

We still observe that the adjoint flux in the highest energy group remains zero because its instream is set at zero and therefore it has no importance. We see that the adjoint flux in the 84^{th} group gains energy from the local adjoint source and will go to zero after the tumour region. Adjoint flux in the 42^{nd} group will gain a lot more energy and reaches its maximum flux at the boundary of the local adjoint source. It gains more energy because there are more neighbour groups that gained energy through the adjoint source.

4.2. Response Changes

To check whether the change in response can be calculated with the help of the adjoint proton flux, we calculated the change in response in two different ways: calculating the Boltzmann proton transport equation, once with initial inputs and once with input changes for the forward case. One can simple calculate the response change by looking at the flux differences. With the adjoint one can calculate response changes with equation 2.2.14. These two types calculations are compared with one another.
We chose to vary the total cross section σ_t. Initially setting the total cross section to $0.025cm^{-1}$ and change its value with ±1%, ±5% and ±10%.

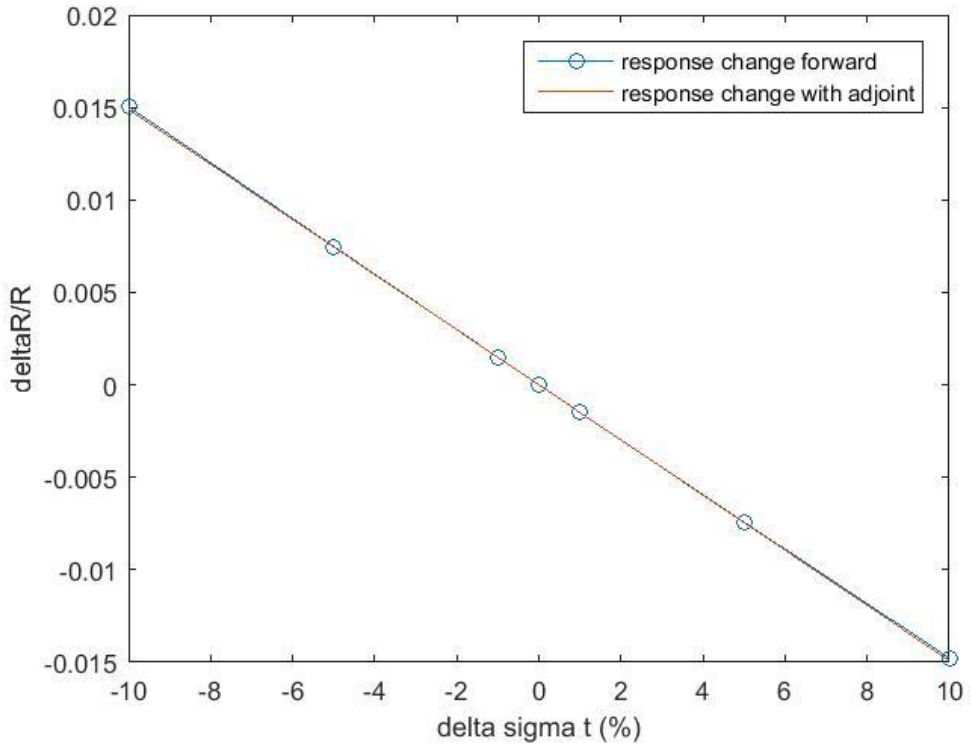

Figure 9: Plot of response changes vs sigma t changes. This calculation is performed with an adjoint source / tumour on the whole domain. (Plot details: 128 energy groups, 128 space elements and 1 angular element μ = -0.7092178)

A response calculation is done with the two different approaches. The response calculation with the help of the adjoint works very well for this type of calculation.

We did the same ΔR calculations for a local adjoint source / tumour around the Bragg peak (space element 70-100). We did this calculation again using the two different approaches. The result that we obtained is plotted in figure 10:

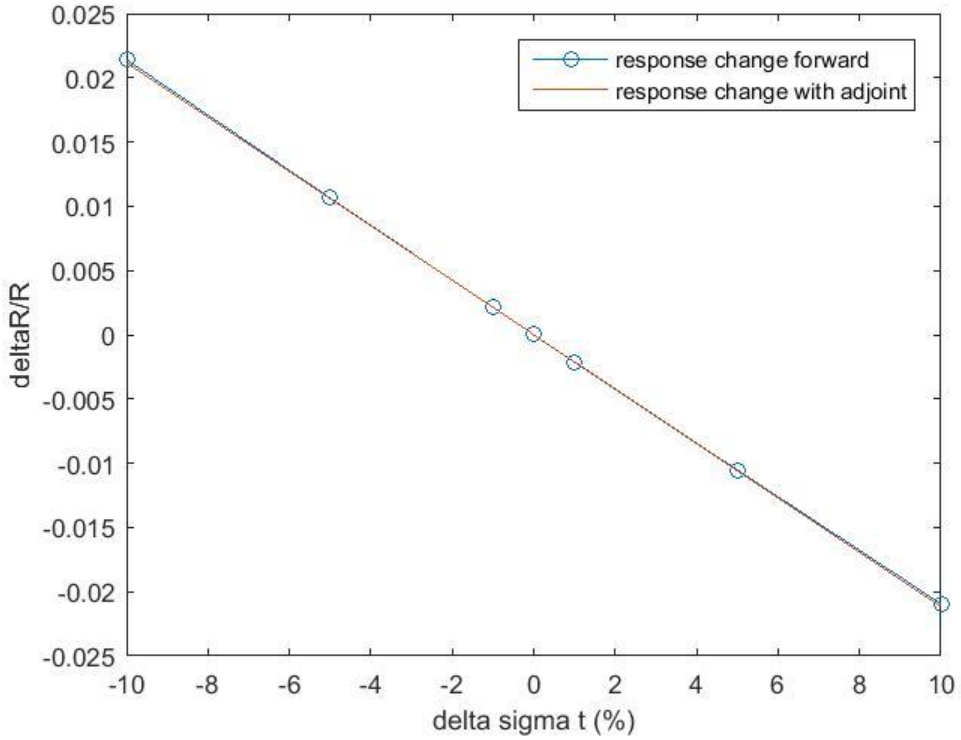

Figure 10: Plot of response changes vs sigma t changes. This calculation is performed with an adjoint source / tumour on the Bragg peak (space element 70-100). (Plot details: 128 energy groups, 128 space elements and 1 angular element μ = -0.7092178)

The response changes calculated with the adjoint flux work well with a local adjoint source. The response calculated with the adjoint flux accurately approaches the response calculated with the forward dose calculations. The difference between the local adjoint source and the adjoint source on the whole space domain can be obtained by looking at the ΔR/R-axis. The response changes with a local source at the Bragg peak are bigger than for the adjoint source on the whole space domain.

5. Discussion and Conclusion

The main goal of this thesis was to test the suitability of adjoint theory for calculating proton doses. Therefore one derived and discretized an equation for the adjoint proton flux and discretize this flux, to implement it into a numerical code and solve it. With this adjoint proton flux one can perform dose and flux calculations much quicker and cheaper, because one can calculate changes in the response, without calculating the change of the flux.
In this chapter one can read the discussion about the main results and conclusions of this thesis. And in the final section of this chapter, we give recommendations and possible improvements for future work.

5.1. Conclusion

To check if the change in response can be calculated with the help of the adjoint proton flux, we calculated the change in response in two different ways. The first way to determine response changes is the regular forward way, by calculating the Boltzmann proton transport equation, once with initial inputs and once with input changes and determine the response changes. One can simple calculate the response change by looking at the flux differences. With the adjoint one can calculate response changes by working out the following derived equation (equation 2.2.14): $-< \varphi^{\dagger}, \Delta B\varphi >$. These response calculations are compared with one another.
We initially set the total cross section σ_t at 0.025cm^{-1} and change its value with ±1%, ±5% and ±10%.
After plotting the response changes for an adjoint source on the whole space domain and for a local adjoint source around the Bragg peak, we can conclude that the response changes can be calculated accurately with the help of the adjoint proton flux. With the necessary improvements calculating response changes with adjoint theory is much faster than forward calculations. Adjoint theory creates an opportunity to do many calculations at once, to decrease uncertainty in locating the Bragg peak. This can improve the future of proton therapy vigorously.

5.2. Future Work

This thesis provides a good basis for future research; however some improvements are needed to implement this technique into practice. In this section, we provide improvements that are or may be needed for more accurate results and practical implementation.
In order to reach the full potential and accuracy of proton transport inside the body, one has to derive the 3D adjoint proton transport equation from the 3D Boltzmann Fokker-Planck approximation. The Fokker-Planck approximation itself is a good approximation, but with every approximation it provides not the actual theoretical value. In this thesis we neglect energy straggling in the continuous slowing down term for simplicity. To reach the best results possible, this term has to be taken into account.

Energy that is transferred to secondary particles must be included in the S_N method. When this is done, one can create a calculation using the typical energy range of proton therapy (70MeV-200MeV).

A 3D calculation of the adjoint source is needed for an exact practical representation. To calculate the 3D adjoint source, one needs the 3D Boltzmann Fokker-Planck proton transport approximation.

In this thesis we have neglected the streaming- and removal terms in energy decomposition to derive an expression for the adjoint source. For more accurate derivation of the energy decomposition, and thus a more accurate derivation of the adjoint source, these terms must be taken into account.
In the expression for the adjoint source we have neglected the $E_{min}S(E_{min})/\Delta E_g$ term that must be added between the two lowest energy boundaries. In future work this term has to be implemented into the numerical code for a slight energy addition inside the lowest energy group.

For simplicity we considered the adjoint flux to be linear inside the energy groups. While this is a reasonable assumption, in practice (adjoint) flux and stopping power cannot be completely linear inside a group. To reach linearity inside energy groups, one need to expand the number of groups, resulting in increase of computation time. In future work one needs to investigate the ideal balance between the number of energy groups and reasonable computation time. Inside the code we have chosen a fitted stopping power. In future work this has to be replaced with the stopping power of water.

In future work, there has to be developed a more accurate way to define the adjoint flux inside the energy groups. A possible improvement for this linear adjoint flux would be to expand the number of basis functions. Expansion of the number of basis functions could decrease the amount of equations to solve or the number of energy groups, and therefore decreases computation time. In future work, the optimal number of basis functions should be evaluated. This evaluation can be done for discretization in the energy domain, spatial domain and angular domain. With a larger number of basis functions we expect a more accurate and faster way of discretizing.

For the discretization of the adjoint proton transport equation and the adjoint source we have used the linear discontinuous Galerkin discretization method. In future work a better, more precise and advanced discretization methods can be investigated for an improvement of the results and a decrease in computation time.
There is also room for improvement to decrease computation time even more. It should be investigated if a larger number of basis functions can provide more accurate results that are computed quicker.

To accomplish proton beam adaptions due to movement of the patient (breathing, slight movement of the body), one need to continuously image the patient during treatment. A computed tomography scan (CT-scan) or a magnetic resonance imaging scan (MRI-scan) can be used to obtain this information. It would be ideal if these scans can capture the exact composition to determine the stopping power inside the tissues. Therefore the program can calculate the change in response and adapt the proton beam automatically. After the performance of these investigations the adjoint proton calculations can be implemented into proton therapy clinics.

References

[1] Cancerresearchuk.org. (2018). *What is radiotherapy? | General cancer information | Cancer Research UK*. [online] Available at: http://www.cancerresearchuk.org/about-cancer/cancer-in-general/treatment/radiotherapy/about [Accessed 5 Jun. 2018].

[2] Duderstadt, J. and Hamilton, L. (1976). *Nuclear reactor analysis*. New York: J. Wiley.

[3] Goldstein, M. (1996). *The Adjoint Monte Carlo - A viable option for efficient radiotherapy treatment planning*. [online] Beer-Sheva, Israel: Nuclear Research Center-Negev. Available at: http://www.iaea.org/inis/collection/NCLCollectionStore/_Public/28/023/28023531.pdf [Accessed 1 Jun. 2018].

[4] Heron, J. (2009). *Diagram of the energy deposit of electrons, photons and protons.*. [image] Available at: http://www.oncoprof.net/Generale2000/g08_Radiotherapie/gb08_rt25.html [Accessed 10 Jul. 2018].

[5] Hesthaven, J. and Warburton, T. (2011). *Nodal discontinuous Galerkin methods*. New York: Springer.

[6] Hoogenboom, E. (2018). *Adjoint Monte Carlo Methods in Neutron Transport Calculations*. [online] Delft: TU Delft, pp.13-15. Available at: https://www.researchgate.net/profile/Jan_Hoogenboom/publication/34734817_Adjoint_Monte_Carlo_methods_in_neutron_transport_calculations/links/02bfe50f6e1f50afac000000.pdf [Accessed 17 Jun. 2018].

[7] Levin, W., Kooy, H., Loeffler, J. and DeLaney, T. (2005). Proton beam therapy. *British Journal of Cancer*, 93(8), pp.849-854.

[8] National Cancer Institute. (2017). *Radiation Therapy*. [online] Available at: https://www.cancer.gov/about-cancer/treatment/types/radiation-therapy [Accessed 1 Jul. 2018].

[9] Pcc.qub.ac.uk. (2018). *Introduction to Fortran 90, QUB*. [online] Available at: http://www.pcc.qub.ac.uk/tec/courses/f90/stu-notes/f90-stu.html [Accessed 9 Jun. 2018].

[10] Physics World. (2016). *Medical physics Archives – Physics World*. [online] Available at: https://physicsworld.com/c/medical-physics/ [Accessed 27 Jun. 2018].

[11] Proton Beam Therapy Scattering vs Scanning Treatment Techniques. (2018). Troisdorf: Probeam, pp.1-2. Available at: https://www.varian.com/sites/default/files/resource_attachments/Proton_Therapy_TreatmentTechniques_0.pdf [Accessed 14 Jul. 2018].

[12] Ronen, Y. (1986). *CRC handbook of nuclear reactors calculations*. 3rd ed. Boca Raton, Fla.: CRC Press, pp.64-84, 134-149.

[13] St. Clair, W., Adams, J., Bues, M., Fullerton, B., La Shell, S., Kooy, H., Loeffler, J. and Tarbell, N. (2004). Advantage of protons compared to conventional X-ray or IMRT in the treatment of a pediatric patient with medulloblastoma. *International Journal of Radiation Oncology*Biology*Physics*, 58(3), pp.727-734.

[14] Uilkema, S. (2012). *Proton Therapy Planning using the SN Method with the Fokker-Planck Approximation*. [online] Delft: TU Delft. Available at: http://test-nest.tnw.tudelft.nl/fileadmin/Faculteit/TNW/Over_de_faculteit/Afdelingen/Radiation_Radionuclides_Reactors/Research/Research_Groups/NERA/Publications/doc/MSc_Sander_Uilkema.pdf [Accessed 27 May 2018].

Appendix

1. Testing Numerical Approach

To check if the numerical approach is coded down the right way a test has to be done. In the code there is an opportunity to turn individual parts of the (adjoint) Boltzmann proton transport equation off. This can be convenient when one wants to test if the new part of the code makes sense.
The streaming- and angular diffusion term are switched off to test the adjoint source and adjoint slowing down. The resulting adjoint equation is as follows:

$$\sigma_t \varphi^\dagger + S(E)\frac{\partial}{\partial E}\varphi^\dagger = S^\dagger. \tag{A.1.1}$$

The adjoint source for a certain region is derived in equation 2.3.12, and only depends on the stopping power which is linear in a group:

$$S(E) = aE + b. \tag{A.1.2}$$

φ is linear in a group and therefore has a linear form:

$$\varphi^\dagger = cE + d. \tag{A.1.3}$$

For the test one has the freedom to choose the coefficients a and b of the stopping power S(E). To test the adjoint source a constant stopping power proves to be intelligent:

$$S(E) = a. \tag{A.1.4}$$

After filling this data in into equation A.1.1, we will end up with this equation:

$$\sigma_t(cE + d) + ac = a \tag{A.1.5}$$

$$\sigma_t cE + \sigma_t d = a(1 - c) \tag{A.1.6}$$

To make sure this equation holds, it follows that $c = 0\ and\ d = \frac{a}{\sigma_t}$, resulting in an adjoint angular flux: $\varphi^\dagger = \frac{a}{\sigma_t}$.

To test the adjoint slowing down term, a linear stopping power is needed. For simplicity we assume σ_t to be zero. Filling this data again in into equation A.1.1, leads to this a new equation:

$$c(aE + b) = aE + b \tag{A.1.7}$$

$$acE = aE + b - bc \tag{A.1.8}$$

From equation A.1.8 this relation follows: $c = 1, d = free\ choice$, resulting in an angular flux: $\varphi^{\dagger} = E + d$.

So for every a and b that in the stopping power equation, an adjoint angular flux in the form of $\varphi^{\dagger} = E + d$ must come out. When this adjoint flux come out of the numerical approach, then one can conclude that the adjoint source and adjoint slowing down terms are coded down the right way. The adjoint flux with only the slowing down term working on it looks like this:

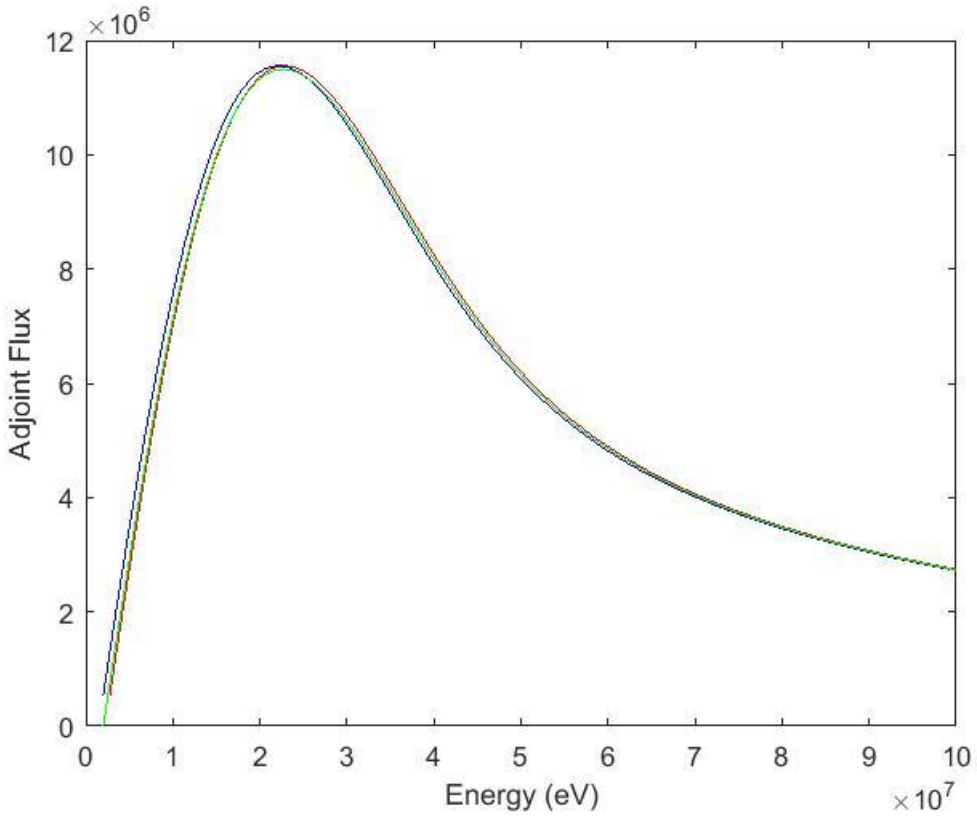

Figure 11: A plot of the energy vs adjoint flux when only the adjoint slowing down works on the flux. Green line represents the slowing down term inside the code. Red and blue line represent theoretical values for lower bound energy and upper bound energy. (Plot details: 128 energy groups, 128 space elements and 1 angular element μ = -0.7092178)